

## ARTICLE

# Layered double hydroxide composite monoliths with three-dimensional hierarchical channels: structural control and adsorption behavior

Cite this: DOI: 10.1039/x0xx00000x

Received 00th January 2012,  
Accepted 00th January 2012

DOI: 10.1039/x0xx00000x

www.rsc.org/

Naoki Tarutani,<sup>a</sup> Yasuaki Tokudome,<sup>a\*</sup> Kazuki Nakanishi,<sup>b</sup> and Masahide Takahashi<sup>a</sup>

Hierarchically porous layered double hydroxide (LDH) materials have potential in anion-exchange, adsorption and catalysis applications, because of their large surface areas and liquid transportation capabilities. The preparation of monolithic LDH-Al(OH)<sub>3</sub> composites with hierarchical μm/nm-scale channels and their adsorption behavior is reported. Monolithic gels were synthesized via sol-gel processing, from metal salt precursor solutions. μm-scale macrochannels spontaneously formed by inducing phase separation during sol-gel transition. nm-scale mesochannels were accommodated as interstices between primary/secondary particles. In this study, these hierarchical channel sizes were controlled. The macrochannel size was controlled by tuning the degree of phase separation. The mesochannel size was controlled independently, by tuning the crystallite size of LDH under different solvothermal conditions. The relationship between pore characteristics and adsorption behavior of tailored hierarchically porous LDH-Al(OH)<sub>3</sub> monolithic gels were investigated by using dye molecules as adsorbates. Monolithic gels with larger macrochannels and mesochannels exhibit faster adsorption rate and higher affinity, respectively. LDH-Al(OH)<sub>3</sub> monolithic gels with hierarchical channels may have potential in some applications such as biosensing, water purification and catalysis.

## Introduction

Layered double hydroxides (LDHs) are ionic lamella compounds. They consist of positively-charged hydroxide sheets, with charge-compensating anions residing in interlayer galleries. Their general formula is  $[M(II)_{1-x}M(III)_x(OH)_2]^{x+}[A^{n-}]_{x/n} \cdot zH_2O$ , where M(II) and M(III) are di- and trivalent cations, respectively,  $A^{n-}$  is the charge compensating anion, and x has a nominal value of 0.2–0.4.<sup>1,2</sup> LDHs are characterized by their anion-exchange properties, adsorption capability and surface basicity. Such properties are controllable because of the compositional diversity of LDHs.<sup>3–5</sup> LDHs have found research application in adsorbent,<sup>6</sup> catalysts,<sup>7</sup> sensors,<sup>8</sup> supercapacitors<sup>9</sup> and drug delivery hosts.<sup>10</sup>

Porous LDH materials exhibit advantages in adsorbent application, because porous structures can improve liquid and molecular/ion transport to internal LDH surfaces. Hierarchical pores of nm and μm sizes are especially desirable, since they are likely to increase the accessible surface area and enhance liquid and molecular/ion transport. Developing controllable pore characteristics of hierarchically porous LDH materials is also important. Adsorption characteristic is likely to be controlled, by optimizing its nm scale pore characteristics to the size of molecules/ions and μm scale pore characteristics to viscosity of liquids in respective applications. Liquid-crystal-templating,<sup>11</sup> bio-templating<sup>12</sup> and hard-sphere-templating<sup>13</sup>

have been used to fabricate porous LDH materials. These routes have all yielded single-sized (not hierarchical), and moreover the fabricated pores are not freely controllable. There are no reports on the fabrication of hierarchically porous LDH material with controllable pore characteristics to date. There have been limited reports on the relationship between pore characteristics and adsorption behavior of LDH crystals, even for those containing single-sized pores. Fabricating hierarchically porous LDH material with controllable pores and investigating its adsorption characteristics will aid its use in innovative and conventional applications.

We recently reported a fabrication pathway for hierarchical porous monolithic LDH gel.<sup>14</sup> The addition of pro-pylene oxide (PO) to a mixture of magnesium chloride hexahydrate (MgCl<sub>2</sub>·6H<sub>2</sub>O), aluminum chloride hexahydrate (AlCl<sub>3</sub>·6H<sub>2</sub>O) and poly(ethylene oxide) (PEO) in ethanol (EtOH)/water produced LDH-Al(OH)<sub>3</sub> composites of cm-scale dimensions. The monolithic LDH gel possessed hierarchical interconnected pores (channels). μm-scale macrochannels spontaneously formed by inducing phase separation during sol-gel transition. nm-scale mesochannels were accommodated as interstices between primary/secondary particles. The monolithic hierarchical channel structure exhibited favorable sorption affinity, upon testing with an aqueous dye. However, independently controlling the pore characteristics of monolithic porous LDH has not been achieved.

Herein, we focus on controlling the characteristics of the mesochannels and macrochannels, of the hierarchically-porous LDH monolithic gel. Macrochannels are controllable by tuning the phase separated structure. Mesochannels are controllable by facilitating the crystalline growth of LDH. These procedures allow the mesochannels and macrochannels to be independently controlled. Adsorption characteristics are investigated using aqueous fluorescent adsorbates, to assess the influence of channel characteristics on LDH adsorption. These results make significant progress on optimizing the channels inside LDH materials. The structural control in this study may further the applications of LDH-based monolithic gels in catalysts, sensors and toxin removal.

## Experimental

**Materials.**  $\text{AlCl}_3 \cdot 6\text{H}_2\text{O}$  (98.0%),  $\text{MgCl}_2 \cdot 6\text{H}_2\text{O}$  (98.0%), EtOH (99.5%), PEO ( $M_w = 1.0 \times 10^6$ ), PO (>99%), 8-hydroxypyrene-1,3,6-trisulfonic acid, trisodium salt (pyranine) and Rhodamine B were used as received. PEO, PO, pyranine and Rhodamine B were purchased from Sigma-Aldrich Co. All other reagents were purchased from Wako Pure Chemicals Industries, Ltd. Ultrapure water of resistivity of  $18.2 \text{ M}\Omega \cdot \text{cm}$  was used in all experiments.

**Methods.** LDH-based monolithic gel was synthesized by the sol-gel method from ionic precursors, as previously reported.<sup>14</sup>  $\text{AlCl}_3 \cdot 6\text{H}_2\text{O}$  (1.58 g, 6.55 mmol),  $\text{MgCl}_2 \cdot 6\text{H}_2\text{O}$  (1.06 g, 5.23 mmol) and PEO (0–0.04 g) were dissolved in  $\text{H}_2\text{O}/\text{EtOH}$  (4.00/3.00 mL) at  $25^\circ\text{C}$ . PO (1.82 mL) was added, and the solution stirred for 1 min to obtain a homogenous sol. The sol was transferred to a polystyrene container, which was sealed and left to stand at  $40^\circ\text{C}$ , to form a wet gel. After aging for 24 h, the wet gel was soaked in 50 mL of isopropyl alcohol (IPA), and subjected to solvent exchange eight times at  $40^\circ\text{C}$ . Some wet gels were transferred to an autoclave pressure vessel, and subjected to solvothermal conditions in 15 mL of IPA at  $180^\circ\text{C}$  for up to 48 h. A monolithic xerogel was obtained by evaporative drying at  $40^\circ\text{C}$ . Samples are named as listed in Table 1, where PEO amount and solvothermal reaction time were used as variables.

**Adsorption behavior.** Samples were calcined at  $500^\circ\text{C}$  prior to testing. 0.2 or 0.3 g of calcined monolith sample was soaked in 10 mL of aqueous pyranine (14.3 mmol/L) or Rhodamine B (4.76 mmol/L), respectively. 10  $\mu\text{L}$  of supernatant was collected after various times, and diluted 200 times with 1 M NaOH or water, for pyranine or Rhodamine B absorption, respectively. Diluents were analyzed by ultraviolet-visible (UV-vis) absorption spectroscopy. The concentration of dyes in solutions was estimated using the Beer-Lambert law.

**Characterization.** Field emission scanning electron microscopy (FE-SEM; S-4800, Hitachi, Japan) was used to observe sample morphologies. Transmission electron microscopy (TEM; JEM-2000FX, JEOL, Japan) at an operating voltage of 200 kV was used to observe sample microstructures. X-ray diffraction (XRD) using  $\text{CuK}\alpha$  radiation ( $\lambda = 0.154 \text{ nm}$ ) on a Rigaku diffractometer (MultiFlex) was used to characterize sample crystal phases. Fourier transform infrared (FT-IR) spectra were recorded from 5000–400  $\text{cm}^{-1}$  at 4  $\text{cm}^{-1}$  resolution, using a FT-IR spectrometer (ALPHA FT-IR spectrometer, Bruker Optik GmbH). Macroporous and micromesoporous characteristics of samples calcined at  $500^\circ\text{C}$  were analyzed by Hg porosimetry (Poresizer 9320, Micromeritics Co., USA) and  $\text{N}_2$  sorption measurements

(BELSORP-mini II, Bel Japan Inc., Japan), respectively. Prior to  $\text{N}_2$  sorption measurements, samples were outgassed under vacuum at  $100^\circ\text{C}$ . The specific surface area was estimated according to the Brunauer-Emmett-Teller (BET) method, and the pore size distribution was calculated using the Barrett-Joyner-Halenda (BJH) method. UV-vis absorption spectroscopy was used to measure the fluorescence intensity of dyes during adsorption tests. The concentrations of pyranine and Rhodamine B in solution were estimated from the Beer-Lambert law, using the peak intensities at 455 and 550 nm, respectively.

## Results and Discussion

**Formation of the LDH- $\text{Al}(\text{OH})_3$  monolithic gel.** The addition of PO to the metal salt precursory solution induced a rapid pH increase in solution. The pH increased from 1.0 to 2.5 within several min, leading to gelation after 18 min of PO addition (Figure S1). The resulting material was a monolithic wet gel. After drying, a cm-scale crack-free monolithic xerogel was obtained, as shown in Figure 1 (a). Bright and dark field TEM images of the monolithic xerogel are shown in Figures 1(b) and (c), respectively.

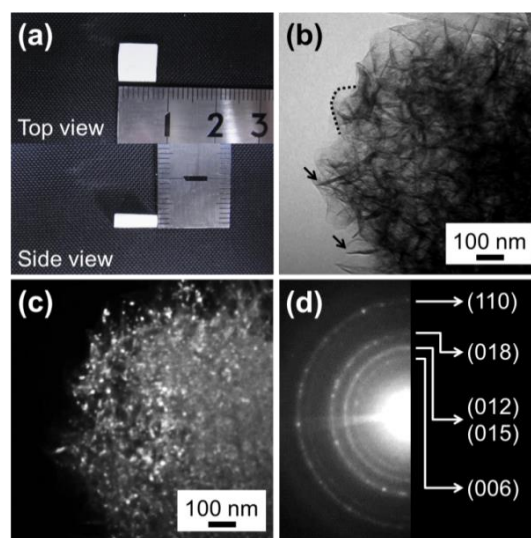


**Figure 1.** (a) Optical, (b) bright field TEM and (c) dark field TEM images and (d) the corresponding electron diffraction pattern of the monolithic xerogel, prepared with 0.03 g of PEO.

The electron diffraction pattern shown in Figure 1(d) inset indicated hydrotalcite-type LDH. This confirmed the formation of LDH, in the xerogel matrix. Figure 1(c) shows a dark field TEM image of the xerogel, using the (012) and (015) diffraction rings of the LDH crystals. LDH exhibiting Bragg diffraction existed as crystalline nanoparticles of diameter < 10 nm, which were homogeneously distributed throughout the xerogel matrix. Fibrous (black arrow) or sheet-like (black dot line) particles  $\sim 100 \text{ nm}$  long of amorphous  $\text{Al}(\text{OH})_3$  were observed in Figure 1(b). Al-rich composition ( $\text{Mg}/\text{Al} = 0.8$ ) suggested that  $\text{Al}(\text{OH})_3$  coexisted with LDH crystals in the obtained gel.  $\text{Al}(\text{OH})_3$  particles have been reported to form fibrous or sheet-like particles, via PO-mediated reactions in Al salt solutions.<sup>15</sup> The results suggested that the monolithic xerogel was a nanocomposite of LDH and  $\text{Al}(\text{OH})_3$ . We previously found its formula to be  $[\text{Mg}_{0.66}\text{Al}_{0.33}(\text{OH})_2\text{Cl}_{0.33} \cdot 2.9\text{H}_2\text{O}] \cdot 3.1\text{Al}(\text{OH})_3$ .<sup>14</sup>

NaOH and urea are basic reagents frequently used to obtain LDH, whereas PO was used in the current study. PO is known to act as a proton scavenger to increase the pH of the metal salt

Table 1. Macrochannel and mesochannel characterization of LDH-Al(OH)<sub>3</sub> monolithic xerogel after calcination.

Sample ID	PEO / g	T <sub>s</sub> <sup>a</sup> / h	d <sub>macro</sub> <sup>b</sup> / μm	V <sub>macro</sub> <sup>c</sup> / cm <sup>3</sup> g <sup>-1</sup>	d <sub>meso</sub> <sup>d</sup> / nm	V <sub>meso</sub> <sup>e</sup> / cm <sup>3</sup> g <sup>-1</sup>	S <sub>BET</sub> <sup>f</sup> / m <sup>2</sup> g <sup>-1</sup>	D <sub>(003)</sub> <sup>g</sup> / nm
P <sub>0.02</sub>	0.02	0	0.29	0.53	8.5	0.45	233	8.0
P <sub>0.03</sub>	0.03	0	0.52	0.75	7.3	0.47	238	7.6
P <sub>0.04</sub>	0.04	0	0.81	0.90	7.1	0.39	226	7.9
S <sub>0</sub>	0.03	0	0.59	0.81	10.1	0.42	184	7.0
S <sub>6</sub>	0.03	6	0.61	0.95	11.3	0.87	359	12.9
S <sub>48</sub>	0.03	48	0.62	0.92	16.8	1.24	415	17.7

<sup>a</sup> Solvothermal reaction time

<sup>b</sup> Pore diameter and <sup>c</sup> pore volume evaluated by Hg porosimetry.

<sup>d</sup> Pore diameter, <sup>e</sup> pore volume, <sup>f</sup> specific surface area evaluated by N<sub>2</sub> sorption measurements.

<sup>g</sup> Crystallite size estimated by the Scherrer equation, from the (003) reflection in the XRD pattern.

precursory solution and lead gelation.<sup>16</sup> To investigate the role of PO in this reaction, NaOH and urea were substituted in its place. Increase rate of the solution pH followed the order of NaOH > PO > urea (Table S1). PO and urea resulted in a homogeneous pH increase, in contrast to NaOH. While LDH was obtained using NaOH and PO, monolithic LDH gel was only obtained using PO (Figure S2). The results indicated that increase rate of the solution pH and its homogeneity were important for obtaining monolithic LDH gel. In the present case, the pH increase induced both coprecipitation and sol-gel transition, to form the composite of LDH and Al(OH)<sub>3</sub>. The solubility of LDH and Al(OH)<sub>3</sub><sup>17</sup> suggested that Al(OH)<sub>3</sub> precipitated in the rapid pH increasing term, within several minutes, after PO addition (Figure S1), and LDH segregated on Al(OH)<sub>3</sub> 'seeds'. This mechanism was supported by results that LDH and Al(OH)<sub>3</sub> formed from solutions containing metal sources of 0 < Mg/Al < 3.0. No solid material (gel or powder) was obtained from Al-free solutions.

**Control of macrochannels by tuning phase separated structure.** Figure 2 shows FE-SEM images of the LDH-Al(OH)<sub>3</sub> xerogels, fabricated from precursors containing different amounts of PEO. LDH-Al(OH)<sub>3</sub> xerogels containing macrochannels formed when the precursor solution contained > 0.02 g of PEO. Figure 3 and Table 1 summarize the macrochannel and mesochannel characteristics of LDH-Al(OH)<sub>3</sub> xerogels fabricated from different precursor compositions and experimental conditions. The macrochannel size could be controlled from 0.3 to 0.8 μm. The obtained xerogels all showed comparable XRD patterns assignable to hydrotalcite-type LDH, and comparable crystallite sizes (Figure S3).

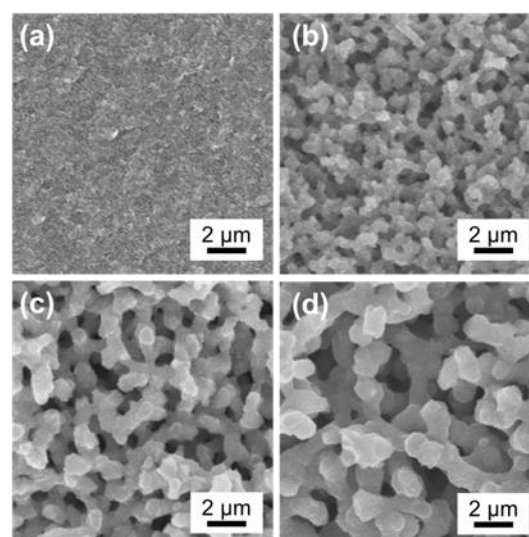


Figure 2. FE-SEM images of LDH monolithic xerogels fabricated from (a) 0.015, (b) 0.02, (c) 0.03 and (d) 0.04 g of PEO.

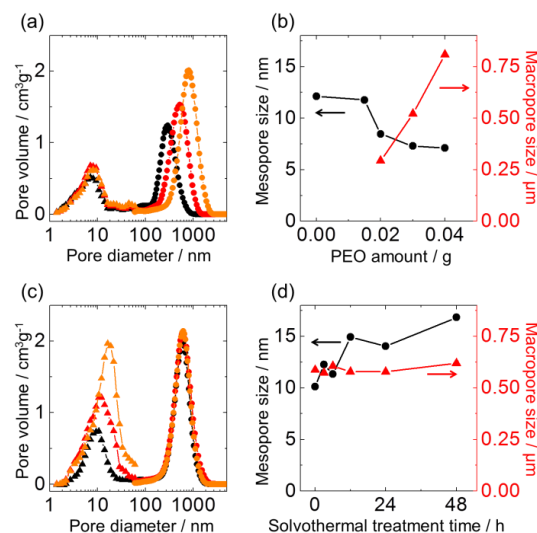
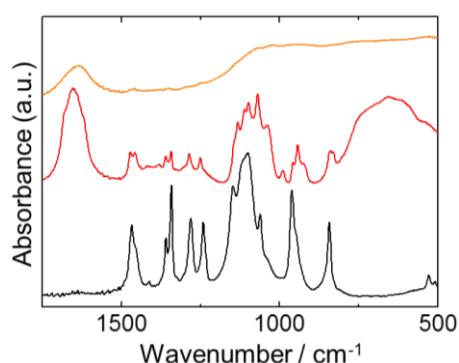


Figure 3. Pore size distributions calculated from N<sub>2</sub> sorption measurements (< 60 nm) and Hg porosimetry (> 60 nm) of xerogels fabricated from different (a) PEO

contents (black: P<sub>0.02</sub>, red: P<sub>0.03</sub>, yellow: P<sub>0.04</sub>) and (c) solvothermal reaction times (black: S<sub>0</sub>, red: S<sub>6</sub>, yellow: S<sub>48</sub>). Mesopore and macropore sizes with different (b) PEO contents and (d) solvothermal reaction times.

Al(OH)<sub>3</sub> precipitated after the addition of PO, and LDH crystals subsequently co-precipitated on Al(OH)<sub>3</sub> particles. The resulting particle size increased with increasing reaction time (Figure S1), reducing the compatibility between LDH-Al(OH)<sub>3</sub> and PEO. This loss of compatibility triggered phase separation, forming domains of LDH-Al(OH)<sub>3</sub>-rich solid phase and PEO-rich liquid phase. In fact, FT-IR spectra indicate that PEO is incorporated in liquid phase, as shown in Figure 4. Spectra were recorded for the solid and liquid parts of the wet gel. The FT-IR spectrum of the liquid part showed absorption bands characteristic of PEO, but no such bands were observed in the spectrum of the solid part. It was concluded that phase separation occurred between LDH-Al(OH)<sub>3</sub> solid phase and PEO-containing liquid phase.



**Figure 4.** FT-IR spectra of PEO (black), dried liquid (red) and solid phases (orange). The two phases were separated each other. Residual components were measured after drying.

Gelation occurred in parallel with phase separation, and the transient phase-separated structure became frozen. Macrochannels formed after removing the PEO-rich liquid phase. The gelation time was independent of PEO content, whereas phase separation strongly depended on PEO content. Thus, a coarser structure was obtained from a higher PEO content, because of the earlier onset of phase separation relative to sol-gel transition. Sol-gel reactions accompanied by phase separation have been employed to produce hierarchically porous monolithic Al<sub>2</sub>O<sub>3</sub>, SiO<sub>2</sub> and TiO<sub>2</sub>.<sup>18-20</sup> However, these reported materials were amorphous. It has generally been difficult to construct monolithic porous structures from crystalline building blocks, because excessive crystallization up to  $\mu\text{m}$  scale size prevents controlling meso/macro pores. The monolithic LDH-Al(OH)<sub>3</sub> composite in the present study is an exception. The  $\mu\text{m}$ -scale three-dimensional architecture was able to be formed, because of the small primary particles formed at a high degree of supersaturation.

**Independent control of hierarchical channels.** PEO content influences on the mesochannel characteristics (pore size and volume) as well as macrochannel characters (Figure 3(b)). An additional procedure was used to independently control the mesochannel characteristics.

The nm-scale structure was controlled by the crystal growth of LDH and Al(OH)<sub>3</sub>. Hydrothermal treatment in an aqueous medium has been reported to induce LDH crystallization,<sup>21</sup> but the macrochannel structure and monolithic shape completely dissolved during hydrothermal treatment. Thus, solvothermal

treatment in IPA was employed to induce LDH crystallization, without excessive dissolution of the monolithic gel. The pore size distributions of solvothermally-treated monolithic gels are shown in Figure 3(c) and (d). Macrochannel sizes were identical, irrespective of solvothermal reaction time. In contrast, the mesochannel characteristics strongly depended on solvothermal reaction time, as shown in Table 1. Mesopore size and volume increased with increasing reaction time. Figure 5 shows XRD patterns of solvothermally-treated monolithic gels. The intensity of the LDH (003) peak ( $2\theta = \sim 11^\circ$ ) increased and sharpened with increasing reaction time, which indicated the enhanced crystal growth. Peaks assigned to AlOOH appeared with increasing reaction time. Solvothermal treatment enhanced the crystal growth of LDH and Al(OH)<sub>3</sub> in the nano-composite. The relationship between crystallite size estimated by the Scherrer equation and solvothermal reaction time is summarized in Figure S4. Increased pore size and volume with increasing reaction time was attributed to the coarsening of mesopores, accompanied with crystal growth during solvothermal treatment. Larger pores remained as accessible channels, even after 50% shrinkage of the wet gel dimensions during drying. This resulted in a large increase in specific surface area with increasing reaction time. In summary, independent control of the mesochannel characteristics was achieved by tailoring the solvothermal treatment conditions.

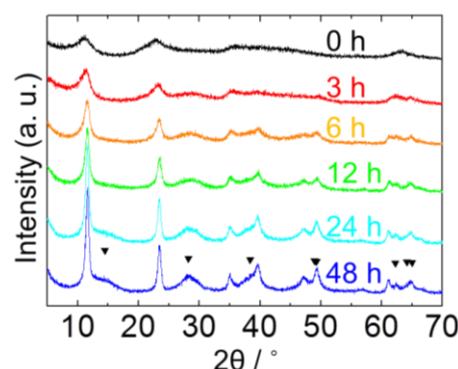


**Figure 5.** XRD patterns of xerogels with increasing solvothermal treatment times.  $\blacktriangledown$ : AlOOH, Boehmite

**Adsorption behavior.** LDH has generally been obtained as a powder in reported studies,<sup>1</sup> and powder molding has been used to fabricate LDH monoliths from LDH powders. Molded monoliths were generally non-porous, which restricted liquid transportation. Available active sites were limited to the outer surface of the molded compounds.<sup>22,23</sup> Introducing hierarchical channels was expected to increase the number of accessible reaction sites. However, fabricating highly porous structures by powder molding is difficult, because increasing the porogen content lowers the mechanical strength, and tends to destroy the monolithic shape. Monolithic LDH-Al(OH)<sub>3</sub> xerogel in this study was sufficiently robust to be used as an adsorbent in the liquid phase, because of the rigidity of its three dimensional connected pore walls. Its interconnected channel structure was favorable for liquid transportation from the outer surface to inner regions, which resulted in a high adsorption capacity per unit sample volume.

Figure 6 shows the time evolution of pyranine adsorption on xerogels with different macrochannel and mesochannel characteristics. Pyranine was selectively adsorbed on the LDH surface, and not on the Al(OH)<sub>3</sub> surface (Figure S5). Figure 6(a) shows pyranine adsorption on P<sub>0.02</sub>, P<sub>0.03</sub>, and P<sub>0.04</sub>. These



three samples possessed similar mesochannel characteristics, as shown in Table 1. Figure 6(a) shows that the monolithic gel with a larger macrochannel size and volume absorbed pyranine more rapidly. Adsorption capacities of the three samples were comparable after 72 h. The macrochannel characteristics had a considerable influence on the adsorption kinetics, with larger macrochannels more easily transporting liquid inside the monolithic gel. Available adsorption sites on LDH were comparable, irrespective to the macrochannel characteristics, as evidenced by the comparable adsorption capacities of the samples after 72 h. The mesochannel characteristics had a negligible influence on the adsorption rate and capacity of pyranine, as shown in Figure 6(b). The results suggested that mesochannels did not enhance the transport of pyranine, and that transport was primarily governed by the macrochannel morphology. In spite of different sample specific surface areas,  $S_0$ ,  $S_6$  and  $S_{48}$  exhibited comparable adsorption capacities after 72 h. This implied that the number of accessible adsorption sites on LDH was comparable for these samples. Increased specific surface area with increasing reaction time was attributed to the increased  $\text{Al}(\text{OH})_3$  surface area. To verify this, Rhodamine B was used as an alternative adsorbate, which could adsorb on  $\text{Al}(\text{OH})_3$  as well as LDH. Figure 7 shows the time evolution of Rhodamine B adsorption on  $S_0$  and  $S_{48}$ .  $S_{48}$  absorbed a larger amount of Rhodamine B, supporting that the increased surface area upon increasing reaction time was due to an increase in  $\text{Al}(\text{OH})_3$  surface area. In summary, larger macrochannels resulted in faster adsorbate transportation, and faster adsorption on LDH. Larger specific surface area samples exhibited a greater Rhodamine B adsorption affinity. Efficient adsorption was achieved on  $\text{LDH-Al}(\text{OH})_3$  with high surface area and large macrochannels, irrespective of mesochannel characteristics. Controllable hierarchical channels demonstrated here allow size-exclusion effects against adsorbates, which could open up various innovative applications. For example, a highly selective adsorbent is expected by taking advantages of macrochannels as protein/cell filters, and mesochannels as biomolecule/nanoparticle filters.<sup>24–26</sup>

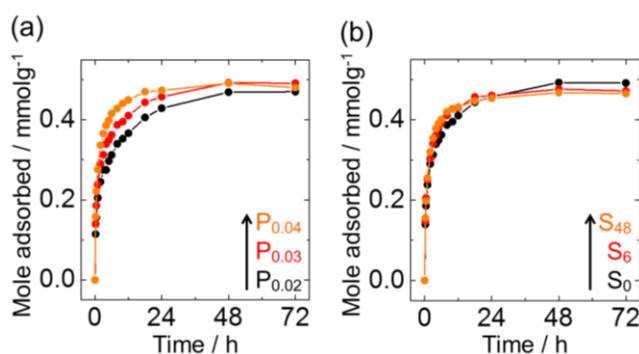


**Figure 6.** Pyranine adsorption on xerogels with different (a) macrochannel (black:  $P_{0.02}$ , red:  $P_{0.03}$ , yellow:  $P_{0.04}$ ) and (b) mesochannel characteristics (black:  $S_0$ , red:  $S_6$ , yellow:  $S_{48}$ ).

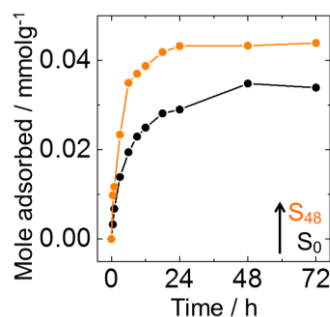


**Figure 7.** Rhodamine B adsorption on xerogels with different mesochannel characteristics (black:  $S_0$ , yellow:  $S_{48}$ ).

## Conclusions

$\text{LDH-Al}(\text{OH})_3$  monolithic xerogels with hierarchical macro/meso channels were synthesized by the epoxide-mediated sol-gel reaction and simultaneous phase separation. The xerogel was a composite of nanoparticulate  $\text{Mg-Al-Cl}$ -type LDH and  $\text{Al}(\text{OH})_3$ . Macrochannel and mesochannel characteristics were independently controlled, by tuning the phase separated structure and improving crystal growth. Xerogels with larger macrochannels exhibited faster pyranine adsorption on their LDH crystals. Xerogels with larger surface areas exhibited higher Rhodamine B adsorption capacities.  $\text{LDH-Al}(\text{OH})_3$  monolithic xerogels with hierarchical channels exhibited controllable adsorption properties, due to their controllable channel characteristics.  $\text{LDH-Al}(\text{OH})_3$  monolithic xerogel reported in this study may have applications in biosensing, toxin removal and catalysis.

## Acknowledgements

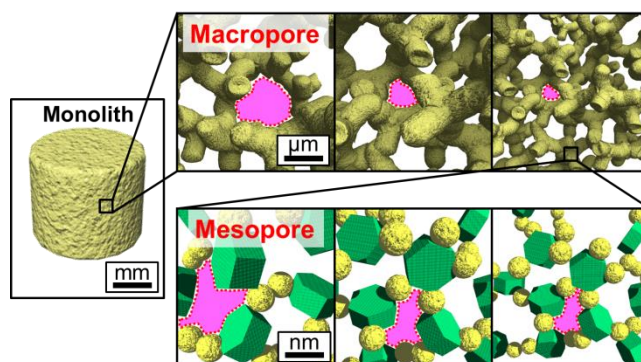
The study was supported by a Grant-in-Aid for Scientific Research (B) (No. 22360276) and a Grant-in-Aid for Young Scientists (B) (No. 24750206), from the Ministry of Education, Culture, Sports, Science and Technology (MEXT), Japan Society for the Promotion of Science (JSPS). M. T. acknowledges financial support from The Murata Scientific Foundation.

## Notes and references

<sup>a</sup> Department of Materials Science, Graduate School of Engineering, Osaka Prefecture University, Sakai, Osaka 599-8531, Japan  
<sup>b</sup> Department of Chemistry, Graduate School of Science, Kyoto University, Kitashirakawa, Sakyo-ku, Kyoto 606-8502, Japan  
 Electronic Supplementary Information (ESI) available. See DOI: 10.1039/b000000x/

- G. Brown and M. C. Gastuche, *Clay Miner.*, 1967, **7**, 193.
- G. W. Brindley, and S. Kikkawa, *Am. Mineral.*, 1979, **64**, 836.
- W. Kagunya, Z. Hassan and W. Jones, *Inorg. Chem.*, 1996, **35**, 5970.
- T. Kameda, S. Saito and Y. Umetsu, *Sep. Purif. Technol.*, 2005, **47**, 20.
- J. Das, B. S. Patra, N. Baliarsingh and K. M. Parida, *App. Clay Sci.*, 2006, **32**, 252.
- B. Bi, L. Xu, B. Xu and X. Liu, *X. Appl. Clay. Sci.*, 2011, **54**, 242.

- 7 G. Busca, U. Costantino, T. Montanari, G. Ramis, C. Resini and M. Sisani, *Int. J. Hydrogen Energ.*, 2010, **35**, 5356.
- 8 W. Shi, M. Wei, D. G. Evans and X. Duan, *J. Mater. Chem.*, 2010, **20**, 3901.
- 9 L. Wang, D. Wang, X. Y. Dong, Z. J. Zhang, X. F. Pei, X. J. Chen, B. Chena and J. Jin, *Chem. Commun.*, 2011, **47**, 3556.
- 10 H. Zhang, D. Pan, K. Zou, J. He and X. Duan, *J. Mater. Chem.*, 2009, **19**, 3069.
- 11 J. Zhao, Y. Xie, W. Yuan, D. Li, S. Liu, B. Zhenga and W. Hou, *J. Mater. Chem. B*, 2013, **1**, 1263.
- 12 Y. Zhao, M. Wei, J. Lu, Z. L. Wang and X. Duan, *ACS Nano*, 2009, **3**, 4009.
- 13 E. Géraud, M. Bouhent, Z. Derriche, F. Leroux, V. Prévot and C. Forano, *J. Phys. Chem. Solids*, 2007, **68**, 818.
- 14 Y. Tokudome, N. Tarutani, K. Nakanishi and M. Takahashi, *J. Mater. Chem. A*, 2013, **1**, 7702.
- 15 T. F. Baumann, A. E. Gash, S. C. Chinn, A. M. Sawvel, R. S. Maxwell and J. H. Satcher, Jr., J. H. *Chem. Mater.*, 2005, **17**, 395.
- 16 A. E. Gash, T. M. Tillotson, J. H. Satcher, Jr., J. F. Poco, L. W. Hrubesh R. L. Simpson, *Chem. Mater.*, 2001, **13**, 999.
- 17 J. W. Bocclair and P. S. Braterman, *Chem. Mater.*, 1999, **11**, 298.
- 18 Y. Tokudome, K. Fujita, K. Nakanishi, K. Miura and K. Hirao, *Chem. Mater.*, 2007, **19**, 3393.
- 19 K. Nakanishi, *J. Porous Mat.*, 1997, **4**, 67.
- 20 J. Konishi, K. Fujita, K. Nakanishi and K. Hirao, *Chem. Mater.*, 2006, **18**, 6069.
- 21 Z. P. Xu, G. S. Stevenson, C. Q. Lu, G. Q. Lu, P. F. Bartlett and P. P. Gray, *J. Am. Chem. Soc.*, 2006, **128**, 36.
- 22 Y. J. Lee, J. S. Lee, Y. S. Park and K. B. Yoon, *Adv. Mater.*, 2001, **13**, 1259.
- 23 Y. Tao, H. Kanoh, L. Abrams and K. Kaneko, *Chem. Rev.*, 2006, **106**, 896.
- 24 Z. Sun, Y. Deng, J. Wei, D. Gu, B. Tu and D. Zhao, *Chem. Mater.*, 2011, **23**, 2176.
- 25 A. Katiyar, L. Ji, P. Smirniotis and N. G. Pinto, *J. Chromatogr. A*, 2005, **1069**, 119.
- 26 T. Hirai, H. Okubo and I. Komasaawa, *J. Phys. Chem. B*, 1999, **103**, 4228.



Layered double hydroxide monoliths with size-controllable macro/mesochannel for adsorbent application.